Advances in Science and Technology Research Journal

Advances in Science and Technology Research Journal, 2025, 19(10), 300–314
https://doi.org/10.12913/22998624/207981
ISSN 2299-8624, License CC-BY 4.0

Received: 2025.06.11
Accepted: 2025.08.15
Published: 2025.09.01

Sheet metal quality measurement using laser speckle method

Sławomir Świłło[1*], Dawid Chojnowski[2]

[1] Faculty of Mechanical and Industrial Engineering, Warsaw University of Technology, ul. Narbutta 85, 02-524 Warsaw, Poland
[2] Keyence International (Belgium) nv/sa, branch in Poland, Bielany Business Point, Irysowa 1, 55-040 Bielany Wrocławskie, Poland
* Corresponding author's e-mail: slawomir.swillo@pw.edu.pl

ABSTRACT

Today's industrial expectation for shaped sheet metal requires the development of new methods for measuring its surface quality. Such solutions need to include both the identification of surface defects and an evaluation of the surface condition after deformation. Therefore, we propose the use of the laser speckle method, a well-known digital-imaging technique. This technique provides a fast and non-contact measurement of the topographical quantities, such as the shape and quality, of manufactured products. In this type of measurement, the laser speckle effect is created when coherent light falls on a rough surface, causing it to scatter randomly. A field of light and dark areas is generated, which directly relates to the geometric structure of the surface. In the solution presented here, stochastic laser speckle analysis was used to determine the correlation between the sheet surface deformation and its quality. For this purpose, optical speckle measurements were carried out on a flat specimen after a uniaxial tensile test. Statistical evaluation of the deformation process demonstrated the applicability of this technique for the quantitative quality control of shaped sheet metal. The measurements were carried out using a specially designed automated optical vision system. Images of the deformed surface were captured by MATLAB software, and second-order statistical features were evaluated using a discrete fast Fourier transform. In addition to the measurements taken, the surface roughness was measured, which provided a full description of the three-dimensional functional geometry of the material being tested. The three-dimensional surface roughness was measured as an important parameter in the surface quality measurement.

Keywords: speckle laser imaging, sheet metal deformation, autocorrelation, Fourier transform.

INTRODUCTION

Modern metal forming places great emphasis on advanced solutions for the efficient design, simulation and modelling of manufacturing processes. Constantly emerging new goals and challenges in this field allow plastic forming to maintain its high position among other manufacturing techniques. The popularity of this technology is evidenced by the fact that, statistically, 90% of a car consists of components formed by metal forming processes [1]. A special example of a technological solution for metal forming is the sheet metal stamping process.

This process involves bending and stretching the material using presses and tools in the form of dies. Compared to other technologies, such as casting, forging or machining, stamping allows the rapid shaping of lightweight products with complex shapes. Hence the widespread use of this method in almost every industrial manufacturing sector, especially the automotive industry [2]. Among the primary challenges of this technology, however, is the pursuit of higher product quality. This process is expected to be improved in the coming years through achievements from the industrial revolution (4.0, 5.0) for every stage of the manufacturing technology, particularly quality control [1]. The following factors favour this development:

- current environmental challenges associated with the ever-increasing demand to reduce negative environmental impacts;

- the need for continuous cost minimisation and the implementation of more-advanced geometric product designs;
- the need for innovative solutions in measurement technologies;
- production constraints on variable working conditions, the environment or the instability of the technological parameters in the production process; and
- the need to safely and effectively achieve the desired goals.

There being a need to accurately identify expectations for the creation of innovative quality-control solutions, it is worth describing these factors in more detail. First, it is important to highlight the ever-increasing expectations for improving the environmental impact of manufacturing processes and products in the automotive sector. European Union environmental recommendations strongly emphasis eliminating greenhouse gases [3]. This has led to a search for lighter and safer car designs, based on aluminium alloys and advanced high-strength steels [4]. The use of new materials poses new forming challenges, such as the greater tendency for material wrinkling due to a lack of adequate tool pressure and a local reduction in sheet thickness. This makes the process of inspecting the condition of the material much more difficult and points to the need for improved solutions in this area.

Second, as recent research [5] has indicated, the nature of damage to advanced high-strength steels is very rapid and there is no localised neck before fracture. This makes it much more difficult to eliminate the hazards that limit the correct course of sheet metal forming based on the forming limit diagrams [6] used in computer simulations of manufacturing technologies. Questions have therefore been raised about the applicability of conventional forming limit diagrams for these new steels because they can lead to incorrect and misleading interpretations [7].

Third, it should be noted that in industrial sheet metal forming technology, surface defects, such as cracking, rippling or local rubbing, are very common [8]. This is often the result of small changes in the process execution conditions (lubrication, temperature or variation in the material strength parameters) due to different suppliers or storage methods. This variability in the material and process properties during metal forming in mass production has a major impact on production accuracy. In the case of mass production, from simple bending operations to the stamping of auto body parts, significant variability has been observed between products. Therefore, numerous statistical analyses have been proposed for the measurement of product geometry and process force measurements. This is because it has been shown that they can be used to directly estimate the variability in product properties using data correlation methods [9].

Fourth, high consumer expectations for quality and safety are making die designs increasingly complex, with sharp edges and rapid curvature changes [10]. Materials, in turn, being more robust, require new alloying solutions. Therefore, today's challenges for sheet metal forming processes are primarily the tight tolerances imposed by contractors, resulting from the assumed geometry of the product.

Thus, manufacturing defects are often encountered, despite advanced computer modelling work on manufacturing processes, carried out as early as the design stage, aimed at determining optimal process execution conditions. Indeed, the quality of the parts formed from sheet metal is strongly dependent on the sheet material used, the coating and tooling material, lubrication and the process conditions. Although friction plays a key role, it is currently not considered in detail in the computer modelling of sheet metal forming [11]. In addition, most approaches to sheet metal forming control focus only on controlling the forming process and optimising the press parameter settings, rather than controlling the quality of the final product [12]. The lack of precise modelling of such complex process conditions is due to the factors mentioned earlier—varying production conditions, the condition of the material, complex product shapes and high tolerance requirements – which leads to increased costs and production downtime [13]. The solution is the idea of Industry 4.0 and 5.0, which enables connectivity through embedded electronics, software, sensors and network communications. This allows data on specific product or process attributes to be exchanged via the Internet to improve overall production efficiency [14].

As a result, real-time monitoring of the condition of shaped products is crucial for the quality and efficiency of industrial processes. Developing an effective solution for eliminating defective products during the plastic forming process seems crucial not only for optimising the tool geometry

at the initial stage of the process, but also for efficient production. This leads to a reduction in the number of non-conforming products. Interest in the development and exploration of state-of-the-art metal forming control systems has increased in the last decade, partly as a result of the Fourth Industrial Revolution, which promotes the use of information systems in modern factories [15]. This makes it possible to create fully automated production lines equipped with devices for the continuous monitoring of manufactured products.

Here, we propose a sheet metal quality-control technique using an automated vision system for use during the industrial inline stamping of auto body panels. For industrial mass production, shaped parts, such as body panels, can be produced at high speed and low cost. Each part is made by placing the sheet metal between the upper punch (stamp) and the lower punch, which are each other's geometric negatives. The punch presses the initial sheet, forming the desired shape, while the blank holders control the delivery of the sheet to the die area. One of the main quality factors in the sheet forming process is deformability, the exceeding of which leads to fracture. The opportunity brought by the proposed measurement technique makes it possible to eliminate potential defects by signalling the phase that precedes cracking.

BACKGROUND

Due to the great importance of the stamping process in the automotive sector, research has mainly been aimed at developing industrial applications for studying the surface condition of shaped sheet metal [16, 17], with cracks that form on the surface during forming being of continuing interest to the industrial sector. Among the oldest known crack identification techniques is the acoustic signal analysis method. An increase in acoustic emission activity is observed throughout the metal forming process [18] and analysis of this can be used to monitor the forming process in real time. This allows the process to be starred with feedback to take advantage of optimal strain values [19, 20].

Another method involves the use of a magnetic sensor to measure the magnetic fields generated during stamping. Using neural networks in magnetic-field imaging, as part of this approach, can lead to automation of the crack signal acquisition process [21, 22]. The detection of surface defects using neural networks is an increasingly common computational activity in the identification of abnormal runs in product manufacturing technology. Neural networks can extend the possibilities of the results obtained by this method by determining the potential causes of the defects. This process involves assigning a detected defect to a similar image stored in the system's memory (crack library). Then the system makes an inference about the defect category based on the appearance of the defect. Hence, the system for detecting defects on the surfaces of shaped sheet metal becomes a combined process of detection, localisation and classification [23, 24].

Industrial applications for the early prediction of the phases preceding material fracture are another method for detecting surface defects, including the early detection of the location of large plastic deformations [25]. In [25], during the sheet metal forming process, the spectrum of radiation in the infrared band was tracked to obtain an image of the distribution of deformations caused by the temperature change on the surface of the deformed sheet, which ultimately led to the early nucleation of cracks.

Industrial conditions mean that any proposed solutions must accommodate the unusual nature of the measurement environment, such as difficulties in accessing the measurement space due to the limited working range of the testing equipment, the need to present results online, and the dynamically changing lighting conditions resulting from interference due to microcracks in small particles on the surface between the sheet and the matrix (emitting a wave of similar frequency to the material) and image interference due to emerging light reflections on the surface of the sheet [26]. This means it is important to search for better solutions, with vision methods being the most widespread [27]. Machine vision methods are commonly used in industry for automatic image processing to extract information critical to the task at hand, a primary task being the process of industrial inspection with particular emphasis on product quality analysis [28]. The primary source of information is, of course, the image obtained from the light reflected from the object, with various sources (e.g. LED, fluorescent, coherent) and types (e.g. direct, angled, reflected) of illumination employed. Vision methods for measuring surface defects in sheet metal forming processes mainly involve the analysis of material test results and the industrial application

of the findings in quality control. The results from laboratory tests aimed at developing methods for predicting cracks in materials are mainly used in the development of limit deformation curves. These are based on the correlation of images recorded during the course of the shaping process and use the dynamic effect of changes in reflected light. Although the recording process itself takes place during deformation (inline), its analysis is carried out after a long delay (offline), which is not crucial for the description of the process. In industrial measurements, however, testing is mainly aimed at determining the condition of the surface after the moulding process (hence, quality control). In industry, due to the measurement conditions (closed moulding space due to the die stamping technology), the surface is available for only a short time, and only after the process has been completed (offline). By contrast, an analysis of the results is required immediately (online), due to the belt production process, contrary to what happens in the laboratory situation.

Thus, laboratory measurements evolved to include methods that use the dynamic speckle effect to analyse the laser spots recorded in images captured by a camera to locate cracks in stamped sheet metal [29]. Dynamic laser speckle (also known as laser speckle imaging) refers to the digital image processing of a scattering pattern applied to a rough surface, usually under deformation. After numerical analysis using autocorrelation, full characteristic scatter points can be plotted on a laser speckle activity graph. From this, it is possible to determine the moment of fracture and ultimately locate this in the principal deformation space of the limit deformation diagram [30].

Another method for detecting cracks in the industrial moulding/stamping of auto body parts [31] involves collecting a dynamically changing pattern of spots (due to the rigid movement of the sheet, rather than deformation, as in the other type of method) and analysing this for cumulative images of surface defects. This analysis takes advantage of the fact that geometric irregularities in the defect area are reflected as changes in laser specular intensity. However, due to the ever-increasing expectations of increasing the final quality of the product, methods that allow not only the detection of cracks, but also the determination of the state of the material in the earlier stages of deformation (localisation of deformation, local rubbing) are being sought. Therefore, we propose a geometric analysis of the laser specks themselves, which is commonly used in surface quality control to measure roughness, for example.

Surface roughness is commonly used to characterise the microstructure of a material, especially during machining [32]. In measuring this, the most popular method is the laser speckle method, where selected specular statistical parameters that are sensitive to the type of machining process can be used to classify the machined surface. Increasingly, however, laser speckle analysis is being used in machining processes, where examples of tool condition and material control can be indicated. In the area of tool remanufacturing, the measurement of roll surfaces in the rolling process can be checked and, if necessary, treated during the remanufacturing process [33]. Thanks to laser spot imaging, this non-contact, non-destructive method can also measure surface deformation. One example involved the R_a being determined during the tensile testing of surface quality, the results indicating that the surface roughness increased with increasing plastic deformation [34]. During this test, the homogeneous surface roughness was found to have been caused by plastic deformation, which then formed a concave surface, leading to cracking. This indicates that surface roughness is one of the key factors affecting fracture during plastic forming [35, 36].

As already mentioned, a better understanding of the magnitude of material deformation leads to the prediction of individual process phases based on the assumptions of the limit deformation curve. This is crucial in industrial quality control (in the detection of defective products) during deep drawing. An attempt was therefore made here to determine the magnitude of deformation indirectly based on changes in roughness in a deformed sheet, and a search was conducted to identify correlations between surface parameters, such as the average roughness and the characteristics of laser specks. For this purpose, the average height of the surface deviations in a specific area (parameter S_a, which is equivalent to R_a) was evaluated. The measurement of S_a provides an analysis of a selected area of the tested sheet surface. It was assessed that, in order to better understand the influence of plastic deformation on surface roughness before material fracture, tensile tests be performed and different deformation areas analysed under a three-dimensional (3D) confocal microscope. It was determined that surface roughness increases

proportionally with increasing plastic deformation, which allowed us to conclude that the measurement of sheet metal areas at risk of cracking could be performed using the laser speckle technique. The aim of this work was therefore to initiate deformation measurements in differentiated deformation areas and to determine the possibility of tracking the deformation front based on roughness measurements.

SPECKLE CONTRAST – FIRST-ORDER STATISTICS

Speckle interference—a phenomenon originally studied by Newton—is known from astronomy, where images recording distant stars are disturbed by the different layers of the atmosphere. In the mechanics of materials testing, this phenomenon is used to study defects and surface quality due to the inhomogeneous fracture rate of light incident on a metallic surface [25]. In the method, laser spot patterns are obtained by illuminating a rough surface through a coherent laser light source. This causes both interference phenomena and significant scattering of the laser light, resulting in fields consisting of bright and dark areas. Unfortunately, these phenomena reduce the legibility of the surface compared to traditional illumination.

In general, it can be assumed that, in surface-quality measurements, speckle pattern magnitudes, including first-order statistical properties, are related to surface roughness [37, 38]. However, they are only able to describe brightness fluctuations. Within the framework of the most commonly used speckle method (laser speckle imaging), numerous methods have been used [39, 40] to extract information on the first-order statistical properties, the most popular being contrast analysis, which is usually defined as the quotient of the standard deviation divided by the average intensity of the speckle image [40]. The mean intensity of a polarised speckle pattern is equal to the standard deviation:

$$C = \frac{\sigma_I}{\langle I \rangle} \tag{1}$$

where: and $<I>$ σ_I are the mean value and standard deviation, respectively, of the intensity calculated for all pixels in the image frame. Hence, the standard deviation of the total intensity will be [38]:

$$\sigma_I = \sqrt{\langle I^2 \rangle - \langle I \rangle^2} \tag{2}$$

In the speckle contrast method [41], the recorded speckle images represent the intensity related to the intensity of the incident light. These images are then discretised, and their numerical record is subjected to statistical analysis based on Equations 1 and 2. The speckle contrast coefficient is determined from the calculations,, which makes it possible to find the roughness parameters of the tested surface. The calculation procedure involves the determination of the first-order statistics, which depend only on individual pixels and are independent of neighbouring pixels. The attributes derived from these statistics are the average brightness of the image and its standard deviation, entropy. A slightly different approach applies to the analysis of pixel intensity image texture attributes, in which the combined distribution of grey levels of pairs of pixels is studied. This allows the extraction of a set of entropy, contrast, energy and homogeneity features, denoted by the relative frequency of two pixels. An alternative to the earlier complex statistical calculations is to analyse a binary image to determine its fractal parameters [42]. Processing binary images greatly reduces the computational complexity by placing a greater emphasis on image analysis. In this method, the speckle image textures are segmented after conversion to a black and white image. Counting of the fractal fields shows a linear dependence on the degree of surface roughness. The accuracy is determined by the choice of an appropriate threshold value in the binarisation process.

However, methods based on the statistics of the first-order properties of light intensity (to which the image-processing method for changes in speckle intensity belongs) are insufficient. This is because they lack the ability to obtain complete information about the surface roughness by not allowing the determination of another basic property of the speckle—the roughness of its spatial structure. Therefore, in order to estimate the average speckle size, a normalised autocovariance function is calculated for the pattern of speckle intensity obtained from the observation plane [43, 44]. Hence, we proposes a method for studying the second-order statistical properties, which are described by the scatter intensity correlation function. In this approach, the speckle size parameters are used to determine the quality of the surface.

METHODOLOGY – SECOND-ORDER STATISTICS

In this method, the speckle images are discretised where a transition is made from the time domain to the spatial domain. The speckle contrast feature associated with the light intensity is then calculated and the surface roughness parameters determined. The proposed method of scattering intensity autocorrelation and autocovariance (these terms used interchangeably) involves calculation of the second-order statistical properties [45]. For autocorrelation, the notation takes the following form:

$$cor(\Delta m, \Delta n) \equiv \equiv \langle I(x_m, y_n) \cdot I(x_{m+\Delta m}, y_{n+\Delta n}) \rangle \quad (3)$$

This is because, as defined, autocorrelation and covariance functions describe how one segment of data is correlated with its neighbouring segments on average. Thus, the autocovariance function can be regarded as a measure of the self-similarity of a signal's deviation relative to its average level. Thus, it can be written that the covariance function (responsible for the value of the average pixel size) for the recorded image of laser specks, obtained from the reflection of light from a sheet surface, will have the following form:

$$cov\,(\Delta m, \Delta n) \equiv \equiv \langle (I(x_m, y_n) - \langle I \rangle)(I(x_{m+\Delta m}, y_{n+\Delta n}) - \langle I \rangle) \rangle \quad (4)$$

Where the average contrast of the image, obtained as a bitmap, is, respectively:

$$\langle I \rangle = \frac{I_1 + \cdots + I_{N \cdot M}}{N \cdot M} \quad (5)$$

The covariance and correlation functions are the same, except that for covariance, the averages were subtracted from the input signals. Due to the nature of the speckle patterns obtained (from coherent light measurements), the size of the speckle becomes an important parameter of the speckle. The random distribution of laser spots on an illuminated surface leads to the conclusion that the spots do not have well-defined sizes, so we can only give a measure of the average spot size. It can also be assumed that the dependence in the form of the value of the average spot size is negligible on random scattering. Instead, it is influenced by the coherence of the incident light—that is, the type of laser. It is also influenced by the property of the random surface – that is, the roughness. Both properties assume perfectly coherent light and a surface roughness on the order of, or greater than, the wavelength of the illumination source. It is common under such experimental conditions to study the speckle intensity on a given observation plane by means of the autocorrelation coefficient. This is the relationship (1) obtained from the normalisation process, where the mean for each sample is subtracted and the result divided by the standard deviation. Because of the two-dimensional domain, the values were increased in quadrature:

$$c_{I(\Delta m, \Delta n)} = \frac{cor(\Delta m, \Delta n) - \mu^2}{{\sigma_I}^2} \quad (6)$$

After expanding the expression to the full notation based on the substitution, we get:

$$c_{I(\Delta m, \Delta n)} = \frac{\langle I(x_m, y_n) \cdot I(x_{m+\Delta m}, y_{n+\Delta n}) \rangle - \langle I \rangle^2}{\langle I(x_m, y_n)^2 \rangle - \langle I(x_m, y_n) \rangle^2} \quad (7)$$

where: the value refers to the measure of the 'average width' of the spot and provides a description of the set of rough surfaces. In this way, it can be noted that the equation has its own different interpretation related to Pearson's correlation coefficient.

Starting from the matrix notation of correlation, it can be written that:

$$\langle I(x_m, y_n) \cdot I(x_{m+\Delta m}, y_{n+\Delta n}) \rangle - \langle I \rangle^2 \equiv \equiv \frac{1}{M \cdot N} \sum_{m=0}^{M-1} \sum_{n=0}^{N-1} [I(x_m, y_n) \cdot I(x_{m+\Delta m}, y_{n+\Delta n})] - \bar{I}^2 \quad (8)$$

and

$$\sum_{m=0}^{M-1} \sum_{n=0}^{N-1} \frac{[I((x_m, y_n) - \bar{I}) \cdot (I(x_{m+\Delta m}, y_{n+\Delta n}) - \bar{I})]}{M \cdot N} \equiv \equiv \langle (I(x_m, y_n) - \langle I \rangle) \cdot (I(x_{m+\Delta m}, y_{n+\Delta n}) - \langle I \rangle) \rangle \quad (9)$$

which is ultimately represented by the covariance notation in Equation (1). Through this transformation, the relationship between autocorrelation and autocovariance can be defined as:

$$cor(\Delta m, \Delta n) = \frac{cov(\Delta m, \Delta n)}{{\sigma_I}^2} \quad (10)$$

which represents the aforementioned Pearson coefficient. Thus, another form of the notation for determining the average value of the width of the speculum is [35]:

$$c_{I(\Delta m, \Delta n)} = = \frac{\sum_{m=0}^{M-1} \sum_{n=0}^{N-1} [I((x_m, y_n) - \bar{I}) \cdot (I(x_{m+\Delta m}, y_{n+\Delta n}) - \bar{I})]}{\sum_{m=0}^{M-1} \sum_{n=0}^{N-1} [I((x_m, y_n) - \bar{I})]^2} \quad (11)$$

A much more convenient way of analysing image data is to use the Fourier transform in the calculations. Based on the Wiener–Khintchin

theorem, autocorrelation is simply given by the Fourier transform of the absolute square. For a continuous stochastic process, the autocorrelation function can be reconstructed from its power spectrum using the inverse Fourier transform.

Another interpretation of this notation refers to the convolution theorem of two functions [46]:

$$f \times g = DTFT^{-1}[DFTF\{f\} \cdot DFTF\{g\}] \quad (12)$$

where: *DTFT* is the fast Fourier transform for the image of specular I, *DTFT*-1 is the inverse transform and <*I*> is the average value of the speckle image intensity.

The only difference between cross-correlation and convolution is the inversion of the sampling at the input [47, 48]. Discrete convolution and cross-correlation are, respectively, defined as follows (for real signals):

$$(f \times g)[\Delta n, \Delta m] = \\ = \sum_{m=0}^{M-1} \sum_{n=0}^{N-1} f(m,n) \cdot g(\Delta n - n, \Delta m - m) \quad (13)$$

$$(f \times g)[\Delta n, \Delta m] \triangleq \\ \triangleq \sum_{m=0}^{M-1} \sum_{n=0}^{N-1} f(m,n) \cdot g(n + \Delta n, m + \Delta m) \quad (14)$$

The cross-correlation of a signal with itself gives its autocorrelation:

$$(I \times I)[\Delta n, \Delta m] \triangleq \\ \triangleq \sum_{m=0}^{M-1} \sum_{n=0}^{N-1} I(m,n) \cdot I(n + \Delta n, m + \Delta m) \quad (15)$$

which, ultimately, gives a modified notation of Equation 1, using the Fourier transform:

$$C_{I(\Delta m, \Delta n)} = \frac{FT^{-1}[FT\{I(x_m,y_n)\}^2] - \langle I \rangle^2}{\langle I(x_m,y_n)^2 \rangle - \langle I(x_m,y_n) \rangle^2} \quad (16)$$

As mentioned earlier, an inhomogeneous intensity distribution does not affect the average spot size, as confirmed by numerous previous works, with experimental evidence presented in [49]. More specifically, it has been shown that the spot produced by structured light has the same average size as that produced by plane waves of uniform intensity and constant phase. Proof of this has been provided by comparing the average spot size generated by structured light modes with that generated by wavefronts of constant phase and amplitude. In both cases, the average spot size is almost identical. This demonstrated speckle property allows for speckle applications in surface quality measurements and is of great importance in several speckle-based applications for developing new methods.

SHEET METAL DEFORMATION

In this study, we examined the commonly used industrial steel DC04. The chemical composition of the steel is shown in Table 1. In a sheet-punching operation, standardised specimens with a thickness of 1 mm were prepared and subjected to uniaxial tension. One side of the specimen was spray-painted with a stochastic mesh.

A schematic showing the dimensional characteristics of the specimen appears in Figure 1a. The direction of the tensile load was oriented parallel to the rolling direction. The tensile test was carried out on a standard tensile testing machine at a crosshead speed of 20 mm/min (Figure 1b). In the designed uniaxial tensile test, the process force was recorded by a strain gauge sensor attached to the specimen holder. The strain was then measured using digital image correlation (DIC) for the deformed stochastic mesh image. The vision system used allowed the digital processing of this image and the measurement of deformation through the use of correlation. The essence of this method was to maximise the normalised correlation coefficient based on the following:

$$C_{xy} = \sum_{i=-M}^{M} \sum_{j=-M}^{M} \left[\frac{f(x_i,y_j) g(x'_i,y'_j)}{\bar{f}\bar{g}} \right] \quad (17)$$

where: *f*(*xi,yi*) and *g*(*x'i,yj'*) are the greyscale images for the points (*xi,yi*) and (*x'i,y'*$_j$), respectively, representing the image before and after deformation, while $\bar{f}$ and $\bar{g}$ define the average greyscale based on the following respective notations:

$$\bar{f} = \sqrt{\sum_{i=-M}^{M} \sum_{j=-M}^{M} [f(x_i,y_j)]^2} \quad (18)$$

$$\bar{g} = \sqrt{\sum_{i=-M}^{M} \sum_{j=-M}^{M} [g(x'_i,y'_j)]^2} \quad (19)$$

Calculations were performed for greyscale images with defined subareas with designated focal points. The degree of material displacement was evaluated by comparing the next two frames of the recorded image during deformation. High-resolution images were acquired for the calculations, which made it possible to differentiate the analytical features of the image for the stochastic grid. The resolution of the patterns on the

Table 1. Chemical composition of the material

Material	Carbon [%]	Manganese [%]	Phosphorus [%]	Sulfur [%]	Fluorine [%]
DC04	0.055	0.25	0.01	0.008	99.5

stochastic grid was consistent with the resolution of the camera recording the image. The magnitude of the displacement, in the form of vectors u and v for each point of the stochastic grid, was then determined as the difference in pixel coordinates of the centre points of the defined subareas before and after deformation. A high calculation accuracy was obtained, due to the subarea analysis. To implement the described DIC procedure, a program especially designed in the MATLAB environment [50] was used to generate deformation meshes. Finally, the deformations [51] were calculated for a given stochastic pattern (Figure 1c) using the point sieves generated from the DIC procedure. In calculating the kinematics of the uniaxial tensile process, the mesh analysis method was used, taking into account the influence of the nearby environment. In mathematical terms, this means the directional derivative of the displacement gradient was used. The successive surroundings of the considered point are understood as the nearest surroundings of the measuring node. The directional derivative of the displacement vector was calculated for the selected point—measurement node $x_i^{(n)}$ from the neighbourhood of point x_i:

$$v_j^{(n)} \Delta u_{i,j} = \frac{\Delta u_i^{(n)}}{\Delta s^{(n)}} \tag{20}$$

where: $\Delta u_i^{(n)}$ is the first order increment of the displacement vector, $\Delta s^{(n)}$ is the distance between points $x_i^{(n)}$ and x_i in the direction $-n$, $v^{(n)}$ expresses the vector cosines of the direction $-n$ and superscript (n) indicates the selected direction.

The displacement increments $\Delta u_{i,j}$ are unknown in this equation. The equation is solved when at least two directions are studied and the method of least squares is used.

CHARACTERISATION OF THREE-DIMENSIONAL TOPOGRAPHY FROM OPTICAL MEASUREMENTS

The surface roughness from optical measurements allowed a complete description of the geometry of the 3D functional parameters of the studied material, such a S_a (Figure 2), as an important indicator in the measurement of quality for which there are numerous solutions based on the measuring apparatus, and especially when it comes to

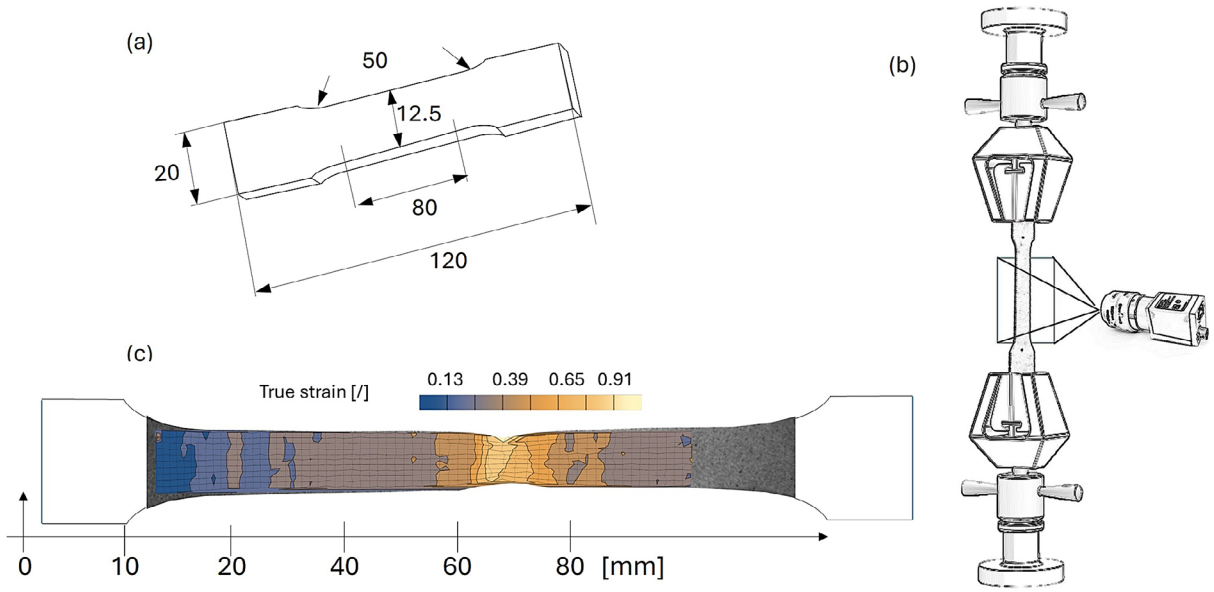

Figure 1. Results of uniaxial tensile test and strain measurement: (a) schematic of the test specimen; (b) tensile system; and (c) strain measurement results

optical measurements [52]. This example is from a confocal optical microscope that scans surface depth using three different techniques – variable focus, laser light and white light interferometers at a resolution of up to 0.1 nm. Therefore, the nature of the specific machining technology associated with its parameters is crucial in developing a solution and quantifying the textural characteristics of the studied surface. For example, we conducted roughness measurements on four areas using a confocal laser microscope (404 nm wavelength, violet laser) of the VK3000 Keyence series. Images were taken in micro mode at magnification (20x/50x) and in laser and optical modes (differential interference contrast). A highly deformed surface (neck area) and a surface without deformation (after sheet rolling) were measured.

From these 3D surface profiles, it was found that the roughness values increased in the area of intense deformation (the neck area). The initial roughness values (S_a = 1.2 μm) (Figure 2a) for the undeformed surface resulted from the rolling process. The basins and hills, visible in Figure 2b,c, take on the character of sharp edges and slopes as they deform, reaching values of about S_a = 4 μm (Figure 2d). Figure 3 shows the behaviour of the surface roughness and the strain changes at the measurement sites. As can be seen, the relationship between these quantities is linear, confirming previous research results [33].

LASER SPECKLE MEASUREMENTS

In the next stage of the study, an experimental measurement of the specimen was carried out in three deformation areas for the inverse surface of the specimen, with no stochastic grid applied. For this, an optical system was used with speckle backscatter imaging (Figure 4a). In this system, a beam of coherent light, with a wavelength of 632 nm and a laser power of 5 mW, created a speckle effect when falling on the rough surface, undergoing random scattering. In order to better visualise the morphology of the studied surface, the optical system included beam splitting through the lens and laser beam scattering (Figure 4b). The laser beam scattering was to minimise the reflections produced by the reflection of the laser light from the surface. In this way, the laser beam scattering from the sample surface selectively suppressed only the specular reflections, resulting in a similar method to the one using orthogonal polarisation between the incident and reflected light [53].

Laser speckle patterns (Figure 4) were obtained by illuminating the rough surface through a coherent source of laser light at a high image magnification (6.5x, ξ = 580 pixels/500 μm) using a RGB–CCD array (640 × 480 pixels) and a pixel size of 5.6 × 5.6 μm^2. Colour image registration allowed for better recording of the pixel images due to the highest sensitivity of the matrix for a length

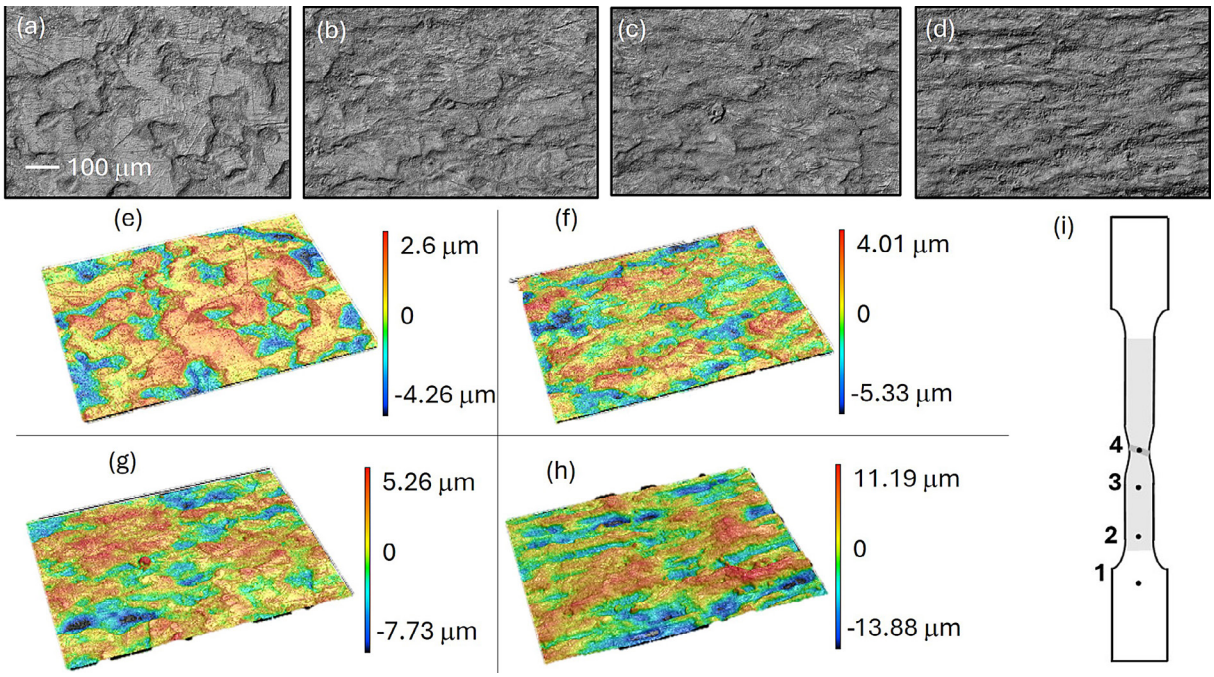

Figure 2. Roughness measurement results—3D view and surface of four regions in the deformed surface area: (a and e) region 1; (b and f) region 2; (c and g) region 3; (d and h) region 4; and (i) regions as shown

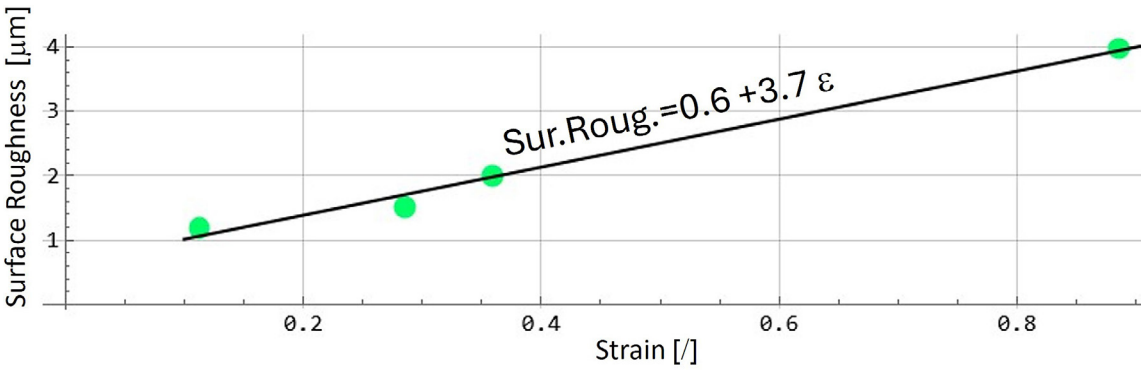

Figure 3. Influence of strain on surface roughness

of 650 µm. To pick up the laser speckle patterns, the waves reflected from the surface passed through a prism system and an adjustable aperture. The optical path of the laser beam was directed to the prism array to make the system more compact for practical applications and independent of the angle of incidence for angular imaging.

DATA ANALYSIS

Moving on to surface quality measurements, we developed a method for optimal laser illumination in relation to exposure time. This method consists of the speckle analysis of a series of measurements from the same point at different illuminations. We determined a certain optimal illumination (local minimum). These measurements on different regions indicated that the size of the speckle clusters varied widely (Figure 5a). The results shown in Figure 5 are based on the average speckle sizes – undeformed surface = 14 pixels, (uniformly) deformed surface = 6 pixels and neck area surface = 3 pixels. Both the interference and significant scattering of the laser light contributed to the observed patterns, leading to the formation of fields consisting of bright and dark areas. The varying magnitudes of these patterns were subjected to statistical analysis, which showed they were directly related to the varying spatial structure (surface geometry). As mentioned earlier, the size of the resulting clusters of speckles became a key parameter. The random distribution of these speckles on the illuminated surface suggested there was no well-defined size, only a measure of the average size of the illuminated areas. Therefore, the average size of these speckles is a measure that characterises the signal sampling requirements.

Figure 5b shows a comparison between the strain and speckle measurements for three selected regions of the test surface. The results are strongly linear. This demonstrates the basis of the method for the resulting minimums and the measurement accuracy. This is because, by scanning a fixed image of the surface using varying exposure times, the minimum speckle size emerges. The emerging minimum may be related to the phenomenon of speckle front growth. In the initial phase of increasing exposure time,

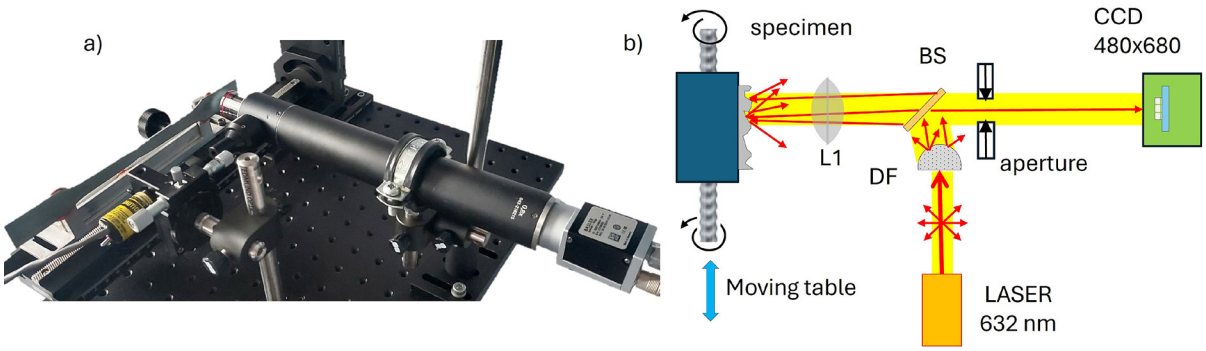

Figure 4. Laser speckle measurement stand: (a) view of the stand; and (b) diagram of the optical measurement system. BS, beam splitting; L1, lens; DF

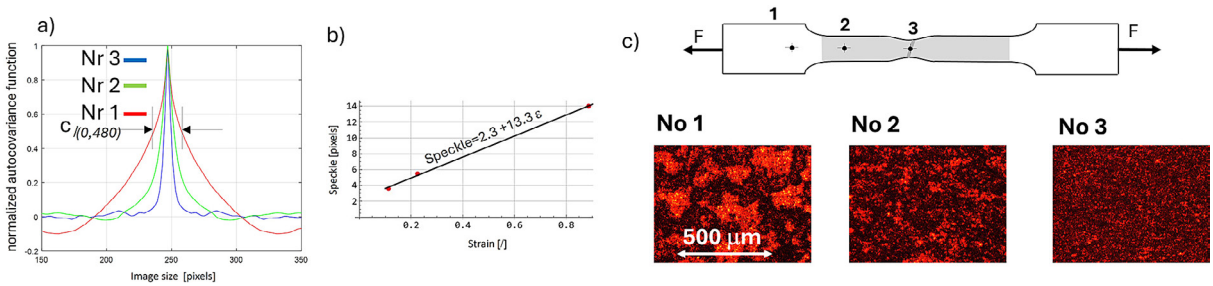

Figure 5. Summary of the autocorrelation results: (a) distribution of speckle size in the specimen cross-section; (b) influence of strain on speckle; and (c) images and locations of speckle measurements

new speckles formed, associated with little visible surface structure, which translates into a decrease in the average value. In the final phase of exposure, the formation of new speckles ended, leading to an increase the size of the already existing speckles. The observed optimal course of the impact of the irradiation provides a positive dimension because it indicates two benefits. First, it shows that the main influence on the size of the average speckle is the speckle build-up front associated with the change in illumination, which minimises the influence of noise. Second, measurements in areas with a large surface quality gradient (change in roughness) require different exposure times, which is not a limitation of the optimal illumination method.

Figure 5c shows images taken on the tensile specimen of the three measurement regions of the speckle. The measurements were located in an undeformed area, an area of low strain with uniform deformation and in the region of intense deformation. The measurements in the region of intense deformation are characterised by the occurrence of a phase of loss of material stability, which is characteristic of the neck. The visible formation of a wrinkle there is a signal of the beginning of material separation. It is therefore the point preceding fracture. However, despite the significant differences in strain in the three selected regions, the characteristics of the dependence of strain on speckle size are linear. Figure 6, shows the results of measuring the variations in optimal illumination for the three test areas. The results were approximated by a second-degree polynomial. The measurements were repeated three times for each area, obtaining deviations in the speckle-averaged values. The largest deviation values (1.5 pixels) were obtained for the undeformed area (region 1). This may be due to the intensity of the reflection of the light from the smooth metallic surface (after sheet rolling)—we did not observe such significant differences for the rough matte surfaces (0.1 and 0.5 pixels).

However, in order to maximise the ratio of the tested signal to the size of the noise, measurements were made at different apertures. This allowed the selection of speckle sizes at which the magnitude of differences between the tested regions of measurements was the largest. In Figure 7, the magnitude of the differences of the measured speckles are shown for two regions (1 and 3). The largest aperture (more light let into the camera, ϕ = 19 mm) produced the largest differences, these decreasing as the aperture decreased (ϕ = 1 mm). In addition, three images of speckles at different apertures (which resulted in different magnitudes of average speckles) are shown for region 3. Estimation of the average

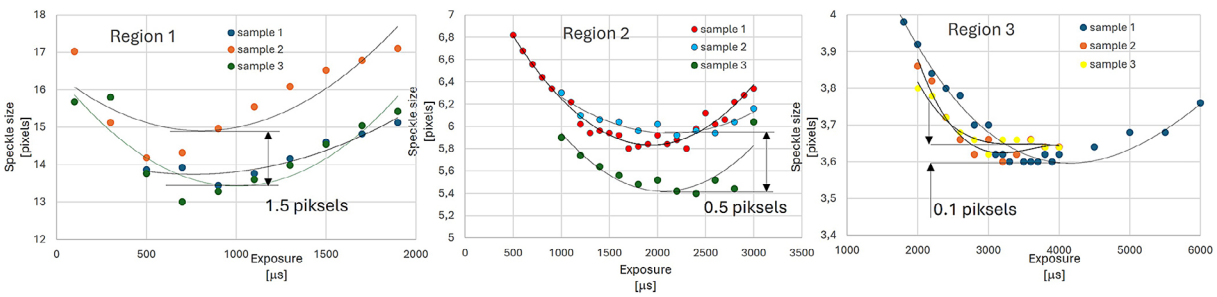

Figure 6. Results of measuring variations in optimal illumination for the three studied regions

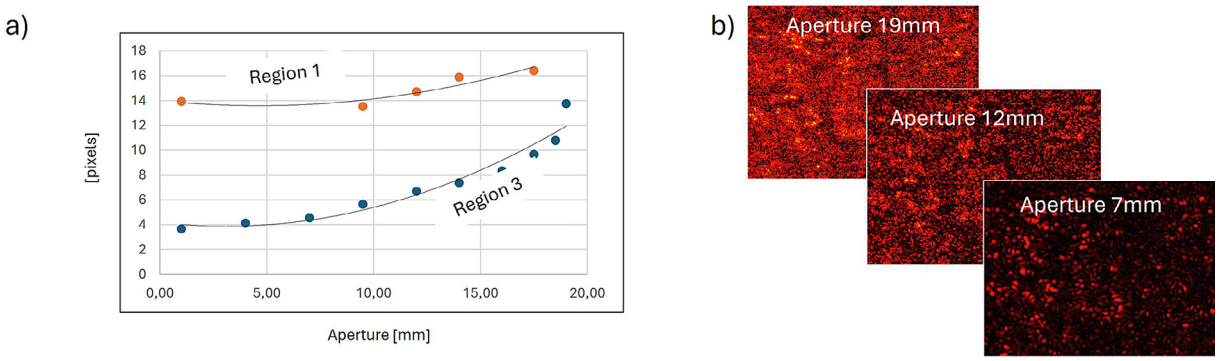

Figure 7. (a) Magnitude of the differences between the measured speckles in two regions (1 and 3); and (b) images of region 3 from the three different apertures

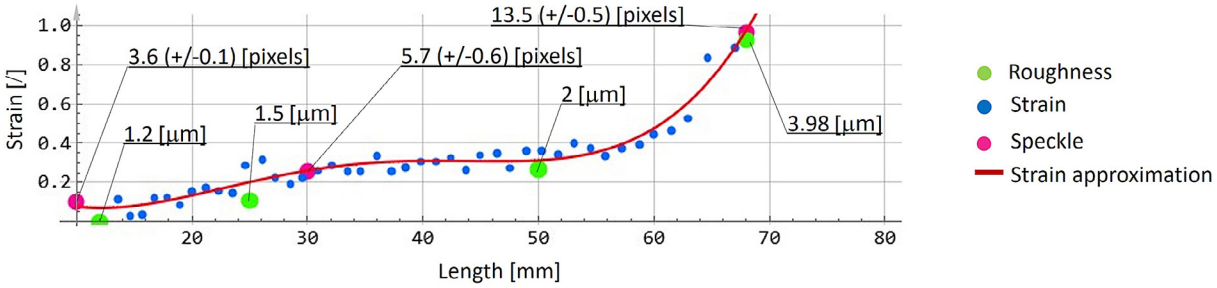

Figure 8. Summary of the speckle and roughness measurements

size of the speckle clusters was calculated using the normalised autocorrelation function for the observed patterns on the studied plane (Eq. 15). The braiding theorem of two functions (Eq. 16) used in this approach allowed a significant simplification of the autocorrelation calculation procedure, written as:

$$c_{I(\Delta m,\Delta n)} = \frac{DTFT^{-1}[DTFT\{I(x_m,y_n)\}^2]-\langle I\rangle^2}{\langle I(x_m,y_n)^2\rangle-\langle I(x_m,y_n)\rangle^2} \quad (21)$$

where: *DTFT* is the fast Fourier transform for speckle image *I*, $DTFT^{1}$ is the means fast inverse transform and <*I*> is the mean value of the speckle image intensity.

The averaged laser speckle size for the area of greatest deformation (low roughness) was characterised by a speckle size of about 4 pixels. This appears to be in line with the recommendation on optimal speckle sizes in [42]. Further adjustment of the aperture increased the speckle size in the undeformed area (from 10 to 5 pixels), resulting in a decrease in measurement resolution at larger apertures. Finally, the results of the speckle and roughness measurements were compared with the strain values in the area of the test specimen (Figure 8). A high linear agreement between the strain and roughness measurements was obtained, confirming previous studies in this area. Similarly, a linear correspondence between the speckle measurements and the strain was obtained, confirming our thesis that the deformation state can be tracked. At the same time, the slight fluctuation in the speckle measurements below +/–1 pixel confirmed the high measurement accuracy of the proposed technique.

CONCLUSIONS

An optical system based on the use of laser back reflection transmission was presented. In this system, two types of laser light scattering were studied—one using a spherical diffuser, the other cross-polarisation. This allowed the capture of changes in the quality of the studied shaped surface based on the phenomenon of speckle formation. During testing, the influence of factors such as sensitivity and resolution of the method was investigated. To study the resolution of the method, the surface quality was measured in a uniform area through a series of trials. The scatter of the results obtained for different magnifications was used to evaluate the ability of the system to accurately assess the surface quality. To examine its sensitivity, a series of measurements

were carried out for a single location at different exposure times.

Summarizing the conducted research in evaluating the quality of shaped metal sheets, the following conclusions can be made:

1. The designed optical system made it possible to record changes in the dispersion of the speckle image under coherent light for the stretched sample.
2. The proposed autocorrelation method makes it possible to indicate changes in the analyzed surface topology quantities accompanying uniaxial plastic deformation.
3. Experimental studies are planned on the applicability of the proposed method in quality control of products obtained by deep drawing of sheet metal. Therefore, it is necessary to check the relationship between the laser speckli method and the strain limit states preceding the cracking of the material.

REFERENCES

1. Gronostajski, Z., Pater, Z., Madej, L., Gontarz, A., Lisiecki, L., Lukaszek-Solek, A., Luksza, J., Mróz, S. Muskalski, Z., Muzykiewicz, W., et al. Recent development trends in metal forming. Archives of Civil and Mechanical Engineering 2019; 19: 898–941. https://doi.org/10.1016/j.acme.2019.04.005
2. Trzepieciński T. Recent developments and trends in sheet metal forming. Metals 2020: 10(6): 779. https://doi.org/10.3390/met10060779
3. European Environment Agency. Trends and Projections in Europe 2023; Publications Office: Luxembourg, 2023.
4. Pereira, R., Peixinho, N., Costa, S. A review of sheet metal forming evaluation of advanced high-strength steels (AHSS). Metals 2024; 14(4): 394. https://doi.org/10.3390/met14040394
5. Bhargava, M., Tewari, A., Mishra, S. K. Forming limit diagram of Advanced High Strength Steels (AHSS) based on strain-path diagram. Materials & Design 2015; 85: 149–155. https://doi.org/10.1016/j.matdes.2015.06.147
6. Wang, K., Carsley, J. E., He, B., Li J., Zhang, L. Measuring forming limit strains with digital image correlation analysis, Journal of Materials Processing Technology 2014; 214(5): 1120–1130, https://doi.org/10.1016/j.jmatprotec.2014.01.001
7. Shi, M.F., Gelisse, S. Issues on the AHSS forming limit determination. In: Proceedings of the IDDRG 2006 International Conference, Porto, Portugal, 2006; 181–188.
8. Hazra, S., Williams, D., Roy, R., Aylmore R., Smith, A. Effect of material and process variability on the formability of aluminium alloys. Journal of Materials Processing Technology 2011; 211(9): 1516–1526. https://doi.org/10.1016/j.jmatprotec.2011.04.001
9. Havinga, J., Van den Boogaard T. Estimating product-to-product variations in metal forming using force measurements. ESAFORM conference, 2017.
10. Manopulo, N., Carleer, B. On the way towards a comprehensive failure modelling for industrial sheet metal stamping processes. IOP Conference Series: Materials Science and Engineering 2019; 651, 012004, DOI: 10.1088/1757-899X/651/1/012004
11. Sigvant, M., Pilthammar, J., Hol, J., Wiebenga, H.J., Chezan, T., Carleer, B., Ton van den Boogaard, Friction in sheet metal forming: influence of surface roughness and strain rate on sheet metal forming simulation results, Procedia Manufacturing 2019; 29: 512–519, https://doi.org/10.1016/j.promfg.2019.02.169
12. Duncan, S. Model based control of product properties: Challenges and Opportunities, In: Forming Technology Forum 2017: 2–4.
13. Havinga, J., Mandal, P., Van den Boogaard, T. Product-to-product state estimation for metal forming mass production, proceedings of Forming Technology Forum 2017: 55–62.
14. Tatipala, S., Wall, J., Larsson, T., Johansson, C., Sigvant, M. Towards Improving Process Control in Sheet Metal Forming: A Hybrid Data- and Model-Based Approach. 2020; 13: 367–377. https://doi.org/10.3233/ATDE200174
15. Thoben, K.D., Wiesner, S.A., Wuest. T. Industrie 4.0 and smart manufacturing-a review of research issues and application examples. International Journal of Automation Technology 2017; 11(1): 4–16. https://doi.org/10.20965/ijat.2017.p0004
16. Tisza, M., Lukacs, Z., Kovács, P., Budai, D. Some recent developments in sheet metal forming for https://doi.org/10.1088/1742-6596/896/1/012087
17. Thuillier, S., Alban, P., Pierre Yves, M. Surface Defects in Sheet Metal Forming: a Simulative Laboratory Device and Comparison with FE Analysis. AIP Conference Proceedings 2011; 1383. https://doi.org/10.1063/1.3623693
18. Miller, R., Hill, E.: Nondestructive testing handbook, acoustic emission testing, 6, ASNT (2005)
19. Baral, M., Al-Jewad, A., Breunig, A., Groche, P., Ha, J., Korkolis, Y., Kinsey, B. Acoustic emission monitoring for necking in sheet metal forming. Journal of Materials Processing Technology 2022; 310: 117758. https://doi.org/10.1016/j.jmatprotec.2022.117758
20. Hao, S., Ramalingam, S., Klamecki, B. Acoustic emission monitoring of sheet metal forming:

Characterization of the transducer, the work material and the process. Journal of Materials Processing Technology 2000; 101 (1–3): 124–136. https://doi.org/10.1016/S0924-0136(00)00441-6

21. Pelkner, M., Kreutzbruck, M. Spin electronics for nondestructive testing. In: Nanomagnetism: applications and perspectives, WileyVCH Verlag GmbH & Co. KGaA, 2017; 81–102. https://doi.org/10.1002/9783527698509.ch5
22. Band, T., Karrasch, B., Patzold, M., Lin, C-M., Gottschalg, R., Kaufmann, K. Simulation-trained neural networks for automatable crack detection in magnetic field images. Journal of Nondestructive Evaluation 2024; 43(19). https://doi.org/10.1007/s10921-023-01034-9
23. Penghua, Z., Seungpyo, J., Yinan, M., Jun, Y. J., and Gyuhae, P. Crack detection on sheet metals using deep learning and a novel data augmentation method (Conference Presentation), Proc. SPIE 12489, NDE 4.0, Predictive Maintenance, Communication, and Energy Systems: The Digital Transformation of NDE, 124890A (25 April 2023); https://doi.org/10.1117/12.2657080
24. Amin, D.,Akhter, S. Deep Learning-Based Defect Detection System in Steel Sheet Surfaces," 2020 IEEE Region 10 Symposium (TENSYMP), Dhaka, Bangladesh 2020; 444–448, https://doi.org/10.1109/TENSYMP50017.2020.9230863
25. Andrianopoulos, N., Champidis, K., Iliopoulos, A. Detection of crack nucleation in sheet metal forming by monitoring infrared radiation. Fatigue & Fracture of Engineering Materials & Structures 2003; 26: 323–328. https://doi.org/10.1046/j.1460-2695.2003.00521.x
26. Machine Vision Algorithms and Applications, Carsten Steger, Markus Ulrich, Christian Wiedemann John Wiley & Sons, 2018.
27. Zhang, H. Machine vision: A comprehensive analysis of techniques, applications, and challenges. Highlights in Science, Engineering and Technology 2023; 71: 299–304. https://doi.org/10.54097/hset.v71i.13050
28. Gayubo, F., González Sánchez, J., Fuente-Lopez, E., Miguel, F., Peran, J.R. On-line machine vision system for detect split defects in sheet-metal forming processes. Proceedings - International Conference on Pattern Recognition 2006; 1: 723–726. https://doi.org/10.1109/ICPR.2006.902
29. Jasiński J., A. Kocańda A. Application of laser speckles to localized necking and cracking detection in Erichsen cupping test, Przegląd Mechaniczny 2014; 9: 49–54.
30. Hu, H., Liang, J., Tang, Z., Guo, X., Li, L. Digital speckle based strain measurement system for forming limit diagram prediction. Optics and Lasers in Engineering 2014; 55: 12–21. https://doi.org/10.1016/j.optlaseng.2013.10.017
31. Świłło, S, Cacko, R. Industrial application of surface crack detection in sheet metal stamping using shift-and-add speckle imaging. Advances in Science and Technology Research Journal. 2023; 17(5): 220–235. https://doi.org/10.12913/22998624/171811
32. Xu, D., Yang, Q., Dong, F. and Krishnaswamy, S. Evaluation of surface roughness of a machined metal surface based on laser speckle pattern. The Journal of Engineering, 2018: 773–778. https://doi.org/10.1049/joe.2018.5057
33. Fischer A.,, Stöbener D. In-process roughness quality inspection for metal sheet rolling, CIRP Annals 2019; 68(1): 523–526. https://doi.org/10.1016/j.cirp.2019.04.069
34. Singh, M, Sharma, S, Muniappan, A, Pimenov, DY, Wojciechowski, S, Jha, K, Dwivedi, SP, Li C, Królczyk, JB, Walczak, D, Nguyen, TVT. In situ micro-observation of surface roughness and fracture mechanism in metal microforming of thin copper sheets with newly developed compact testing apparatus. Materials 2022; 15(4): 1368. https://doi.org/10.3390/ma15041368. PMID: 35207905; PMCID: PMC8877533
35. Zhou, X.H., Su, X. Effects of deformation mode on surface roughening of austenitic stainless steels, Mater. Sci. Technol 2013; 27(6): 1040–1044. https://doi.org/10.1179/026708310X12701095964
36. Ottenklev, F., Adell, M., Orlov, D. Non-monotonic evolution of surface roughness in a stainless steel during cold deformation, Materials Science and Engineering 2021; 799: 140150. https://doi.org/10.1016/j.msea.2020.140150
37. Rodríguez. F., Cotto, I., Dasilva, S., Rey, P., Van der Straeten K. Speckle characterization of surface roughness obtained by laser texturing, Procedia Manufacturing 2017; 13: 519–525. https://doi.org/10.1016/j.promfg.2017.09.077
38. Dainty, J.C., Laser Speckle and Related Phenomena, Springer-Verlag Berlin Heidelberg 1975,
39. Tchvialeva, L., Markhvida, I., Zeng, H., McLean, D.I., Lui, H., Lee, T.K. Surface roughness measurement by speckle contrast under the illumination of light with arbitrary spectral profile, Optics and Lasers in Engineering 2010; 48(7–8): 774–778. https://doi.org/10.1016/j.optlaseng.2010.03.004
40. Postnov, D.D., Cheng, X., Erdener, S.E. Choosing a laser for laser speckle contrast imaging. Scientific Reports 2019; 9: 2542. https://doi.org/10.1038/s41598-019-39137-x
41. Shao, Mq., Xu, D., Li, Sy. et al. A review of surface roughness measurements based on laser speckle method. Journal of Iron and Steel Research International 2023; 30: 1897–1915. https://doi.org/10.1007/s42243-023-00930-8

42. Li, J., Sun, C., Du, Q. A New Box-Counting Method for Estimation of Image Fractal Dimension. IEEE 2006: 3029–3032. https://doi.org/10.1109/ICIP.2006.313005
43. Chicea, D. An alternative algorithm to calculate the biospeckle size in coherent light scattering experiments, Romanian Journal of Physics 2007; 54(1–2): 147–155.
44. Reu, P.All about speckles: Speckle Size Measurement. Experimental Techniques 2014; 38: 1–2. https://doi.org/10.1111/ext.12110
45. Buijs, J., Gucht, J.v.d., Sprakel, J. Fourier transforms for fast and quantitative Laser Speckle Imaging. Scientific Reports 2019; 9: 13279. https://doi.org/10.1038/s41598-019-49570-7
46. Proakis, J.G., Manolakis, D.G. Digital Signal Processing: Principles, Algorithms and Applications (3 ed.) 1996. New Jersey: Prentice-Hall International.
47. Rabiner, L.R., Schafer, R.W. Digital processing of speech signals. signal processing series. Upper Saddle River, NJ: Prentice Hall. 1978; 147–148.
48. Rabiner, L.R., Gold, B. Theory and Application of Digital Signal Processing. Englewood Cliffs, NJ: Prentice-Hall. 1975; 401.
49. Hu, X.B., Dong, M.X., Zhu, Z.H. et al. Does the structure of light influence the speckle size? Scientific Reports 2020; 10: 199. https://doi.org/10.1038/s41598-019-56964-0
50. Eberl, C. Digital Image Correlation and Tracking
51. (https://www.mathworks.com/matlabcentral/fileexchange/12413-digital-image-correlation-and-tracking), MATLAB Central File Exchange. Retrieved March 18, 2022.
52. Świłło, S., Cacko, R. A new approach for evaluation true stress–strain curve from tensile specimens for DC04 steel with vision measurement in the post-necking phases, Materials 2023; 16(2): 558. https://doi.org/10.3390/ma16020558
53. Wang, H., Chi, G., Jia, Y., Ge, C., Yu, F., Wang, Z., Wang, Y. Surface roughness evaluation and morphology reconstruction of electrical discharge machining by frequency spectral analysis, Measurement 2021; 172: 108879. https://doi.org/10.1016/j.measurement.2020.108879
54. LePage, W.S., Daly, S.H., Shaw, J.A. Cross polarization for improved digital image correlation. Experimental Mechanics 2016; 56: 969–985.